Size effects in microstructured superconductors and quantum materials

Fermin, R.

JOSEPHSON PHYSICS IN THIN FILM PLANAR JUNCTIONS

1

2

SUPERCONDUCTIVITY AND JOSEPHSON PHYSICS

Since all chapters in this thesis, except one, concern superconductivity and Josephson junctions, these concepts need some introduction. In this chapter, I will describe that a superconductor is characterized by a transition from fermionic to bosonic behavior of the charge carriers, which leads to a macroscopic quantum state that drives currents by the quantum mechanical phase, expels magnetic fields from the bulk, and exhibits zero electrical resistance. I will discuss the allowed symmetries of the paired electrons and conclude by introducing Josephson junctions and their response to a magnetic field. A part of this chapter is based on the excellent course material on applied superconductivity by Rudolf Gross and Achim Marx[1].

2.1. A MACROSCOPIC QUANTUM PHENOMENON

In a normal metal, charge is carried by electrons. These elementary particles are fermions and thus cannot occupy the same quantum state. Rather, they fill up k-space; therefore, finding a wavefunction that describes such a fermionic system is far from trivial. Including electron-electron interactions, this typically involves solving for 10^{23} degrees of freedom. The quantum mechanical description of a solid radically changes once it enters the superconducting phase. In a superconductor, the electrons experience an attractive force, below a *critical temperature* (T_c), which introduces pairwise phase-coherent interactions between them. These pairs are called *Cooper pairs* and can be regarded as composite particles that are bosonic of nature, which allows them to condense into a single ground state, forming a Bose-Einstein condensate. Since the distance over which electrons pair up is typically much larger than the average distance between electrons, this condensate can be regarded as a fluid, where we think of a density of Cooper pairs instead of individual particles. In this case, the condensate can be captured by a rather simple wavefunction Ψ that describes the collection of all Cooper pairs on the macroscopic scale:

$$\Psi(\boldsymbol{r},t) = \sqrt{n_s(\boldsymbol{r},t)}e^{i\gamma(\boldsymbol{r},t)} \tag{2.1}$$

Here n_s is the density of Cooper pairs, which is equal to the expectation value of Ψ ($|\Psi|^2 = n_s$), i is the imaginary unit, and γ is the phase of the wavefunction. By combining the Schrödinger equation and Lorentz's law, it can be shown that a current density of charged particles $\boldsymbol{J}$, driven by an electromagnetic field, equals[1]:

$$\boldsymbol{J} = q\,\mathrm{Re}\left(\Psi^*\frac{\hat{P}}{m}\Psi\right) = q\,\mathrm{Re}\left(\Psi^*\left(\frac{\hbar}{mi}\boldsymbol{\nabla} - \frac{q}{m}\boldsymbol{A}\right)\Psi\right) \tag{2.2}$$

Here $\hat{P}$ is the momentum operator, q is the charge of the particle, m its mass, $\hbar$ the reduced Planck constant, $\boldsymbol{A}$ is the vector potential and Re indicates the real part the argument. Filling in the wavefunction of Eq. 2.1 yields (omitting the space and time dependencies):

$$\boldsymbol{J} = -\frac{n_s q^2}{m}\left(\boldsymbol{A} - \frac{\hbar}{q}\boldsymbol{\nabla}\gamma\right) \tag{2.3}$$

Realizing that for Cooper pairs $q = -2e$ (twice the electron charge e), and defining $\Phi_0 = \frac{h}{2e}$, the *magnetic flux quantum*, we can write

[1] This is the quantum mechanical analogue of $\boldsymbol{J} = q\boldsymbol{v}n_s$.

$$\boldsymbol{J} = -\frac{\Phi_0}{2\pi\mu_0\lambda_{\mathrm{L}}^2}\left(\frac{2\pi}{\Phi_0}\boldsymbol{A} + \nabla\gamma\right) \tag{2.4}$$

Here λ_{L} is a characteristic length scale of a superconductor, called the *London penetration depth*. Its meaning will become clear under the application of magnetic field, discussed below. It is defined as:

$$\lambda_{\mathrm{L}} = \sqrt{\frac{m}{4\mu_0 n_{\mathrm{s}} e^2}} \tag{2.5}$$

Eq. 2.4 is called the *second Ginzburg-Landau eqation* and is one of the central results of Ginzburg-Landau theory describing the phenomenology of superconductivity. Interestingly, electromagnetic fields couple to supercurrents by a linear combination of the vector potential and the phase of the wave function. Since J is a gauge-invariant property, and both $\boldsymbol{A}$ and γ are not, we require the quantity between brackets in Eq. 2.4 to be gauge-invariant. Therefore Eq. 2.4 is often written as:

$$\boldsymbol{J} = \frac{\Phi_0}{2\pi\mu_0\lambda_{\mathrm{L}}^2}\theta \tag{2.6}$$

Where θ is the called the *gauge-invariant phase gradient*. Clearly, the macroscopic supercurrents are driven by a microscopic quantum mechanical quantity. Therefore, superconductivity is a direct manifestation of quantum effects on the macro scale.

2.2. THE MEISSNER EFFECT AND ITS CONSEQUENCES

In this section, I will describe two more macroscopic properties that result from the quantum nature of the superconducting phase: the zero-resistance state and the Meissner effect. In order to do so, first note that we can combine two of the Maxwell equations ($\nabla\cdot\boldsymbol{B} = 0$ and $\nabla\times\boldsymbol{B} = \mu_0\boldsymbol{J}$) with some vector calculus to find:

$$\nabla^2\boldsymbol{B} = \nabla(\nabla\cdot\boldsymbol{B}) - \nabla\times(\nabla\times\boldsymbol{B}) = -\nabla\times(\mu_0\boldsymbol{J}) \tag{2.7}$$

By virtue of Eq. 2.4, we can obtain the curl of the quantity $\mu_0\boldsymbol{J}$ in a superconductor, noting that the curl of a gradient is zero:

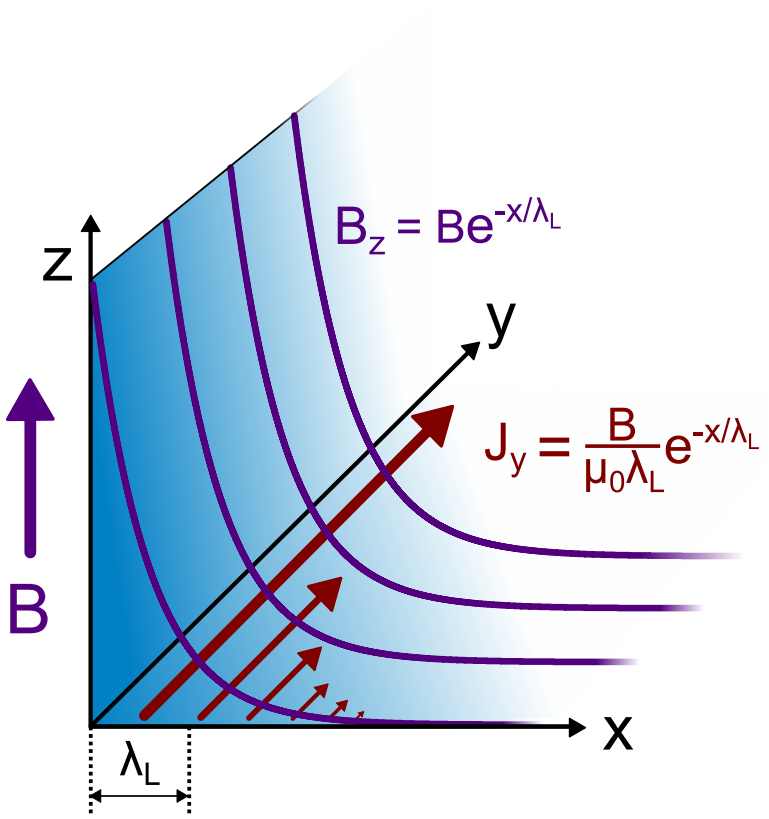

Figure 2.1: Schematic representation of the Meissner effect for a superconductor covering $x > 0$, under an applied field B in the z-direction. Due to the Meissner effect, screening currents run along the boundary of the superconductor, i.e., the y,z-plane. These decay exponentially, giving rise to an exponential decay of the magnetic field in the bulk of the superconductor.

$$\nabla \times (\mu_0 \boldsymbol{J}) = -\frac{\nabla \times \boldsymbol{A}}{\lambda_L^2} = -\frac{\boldsymbol{B}}{\lambda_L^2} \tag{2.8}$$

This Equation is known as the *second London equation*. Combined with the identity of Eq. 2.7, it describes the *Meissner effect*:

$$\nabla^2 \boldsymbol{B} = \frac{\boldsymbol{B}}{\lambda_L^2} \tag{2.9}$$

Clearly, a magnetic field in a superconductor decays exponentially over a length scale λ_L, which can be seen if we solve the differential Equation 2.9 for a superconductor covering the space $x > 0$, subject to a field B in the z-direction (see Figure 2.1):

$$B_z(x,y,z) = Be^{-\frac{x}{\lambda_L}} \tag{2.10}$$

The origin of the exponential decay is a supercurrent that runs along the edge of the superconductor and screens the magnetic field. It is aptly called *screening* or *Meissner current* and is given by $\nabla \times \boldsymbol{B} = \mu_0 \boldsymbol{J}$:

$$J_y(x,y,z) = \frac{B}{\mu_0 \lambda_L} e^{-\frac{x}{\lambda_L}} \tag{2.11}$$

These screening currents play an important role in the discussion on Josephson junctions. Since Eq. 2.8 is known as the second London equation, this naturally leads to the question of what the *first London equation* is. The first London equation is derived using a combination between Lorentz's law and the second London equation; it reads in its linearized form[2]:

$$\frac{\mathrm{d}\boldsymbol{J}}{\mathrm{d}t} = \frac{\boldsymbol{E}}{\mu_0 \lambda_L^2} \tag{2.12}$$

From this Equation, we see that a superconductor can host a stationary supercurrent without the application of an electric field, meaning a zero-resistance state. Interestingly, the first London equation is derived using the second one. This implies that the Meissner effect is a more fundamental property of the condensate than its lack of electrical resistance. The reason why the latter coined the name of the phase can be traced to Heike Kamerlingh Onnes' discovery proceeding that of Walter Meissner. To conclude, the pairing of electrons in Cooper pairs and their entailing change from fermionic to bozonic character directly leads to the expulsion of magnetic fields from the bulk of the solid and the appearance of a zero-resistance state.

2.3. PAIRING SYMMETRY

In section 2.1, I did not discuss the origin of the pairing interaction between the electrons. The microscopic mechanism behind this pairing differs between classes of superconductors and is still the subject of ongoing research, although it is not relevant for the phenomenological description of superconductivity that I present here. However,

[2] Here I have omitted a second term which captures the kinetic energy of the electrons composing the Cooper pairs $\frac{\mu_0 \lambda_L^2 e}{m} \nabla \boldsymbol{J}^2$. This is valid if we assume that the magnetic contribution to Lorentz's law is much smaller than the electric one.

the symmetry of the wavefunction describing a single Cooper pair will be pivotal for explaining its properties in later chapters. Therefore, I will briefly review this so-called *pairing symmetry*.

Although the Cooper pair is a bosonic composite particle, its fundamental constituents are fermionic and, therefore, still obey the Pauli exclusion principle. This implies that the wave function describing the pair must be anti-symmetric under the permutation of the two electrons that make up the Cooper pair, which can best be seen by regarding the anomalous Green's function describing the Cooper pair[2]. It is given by the time-ordered expectation value of two electron annihilation operators[3]:

$$f_{\alpha\beta,ab}(\boldsymbol{r}_1,\boldsymbol{r}_2,t_1,t_2) = \langle \mathcal{T}\, \hat{a}_{\alpha,a}(\boldsymbol{r}_1,t_1)\hat{a}_{\beta,b}(\boldsymbol{r}_2,t_2)\rangle \tag{2.13}$$

The Greek indices here indicate the spin state, the alphabetic indices represent the electron band, $\boldsymbol{r}$ is the position coordinate, and t is the time coordinate of each electron (labeled 1 and 2). Therefore, $\hat{a}_{\alpha,a}(\boldsymbol{r},t)$ removes an electron with spin α from electron band with label a, which is located at position $\boldsymbol{r}$ at time t. Creating a Cooper pair requires two electrons, thus f must be of the form $\hat{a}\hat{a}$. The Pauli exclusion principle states that the electrons cannot be in the same quantum state at equal times ($t_1 = t_2 = t$). Therefore, the Pauli exclusion principle is expressed as:

$$f_{\alpha\beta,ab}(\boldsymbol{r}_1,\boldsymbol{r}_2,t,t) = -f_{\beta\alpha,ba}(\boldsymbol{r}_2,\boldsymbol{r}_1,t,t) \tag{2.14}$$

Anti-symmetry can be expressed by permutation of any of the individual components (spin, spatial coordinate, time, and the electron band of the individual electrons. The latter results in interband or intraband pairing). However, only the total wave function of the pair is required to be anti-symmetric, which lets us classify the pairs on the basis of their underlying symmetries. Figure 2.2 depicts a classification scheme for the allowed pairing states.[3] Below, I will discuss the spin, relative position, and time symmetries in more detail.

The Fourier dual of the relative position between the electrons is their angular momentum. As in the case of electrons orbiting a nucleus, the angular momentum of the Cooper pair is described by a quantum number L. Each of its integer values is assigned a letter, i.e., *s*, *p*, *d*, *f* etc. and is subsequently called L-wave (e.g., *s*-wave). This notation is borrowed from molecular physics and was chosen due to the similarity between the shape of the superconducting gap structure and atomic orbitals. *s*-wave and *d*-wave pairs are symmetric and *p*-wave and *f*-wave are anti-symmetric.

[3] Creation and annihilation operators are part of the second quantization formulation of quantum mechanics, used in describing BCS theory.

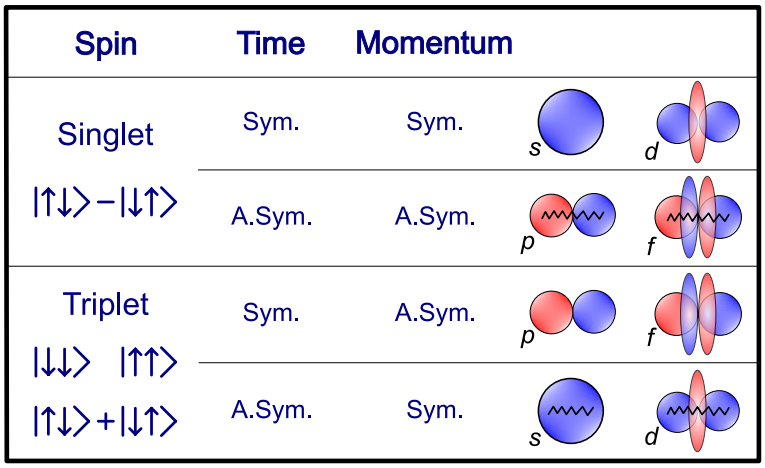

Figure 2.2: Overview of allowed pairing symmetries based on the Pauli exclusion principle. The wavefunction of the Cooper pair is required to be anti-symmetric under the permutation operation, which can result from either the spin, time, or momentum component of the wavefunction. All pairing symmetries can be classified as either spin singlet (S=0) or spin triplet (S=1). The schematics show the resulting allowed pairing symmetries in the last two columns. Here the letter denotes the angular momentum quantum number (Fourier dual of relative position), and the oscillating lines indicate an anti-symmetric time component of the wavefunction. Note that anti-symmetry can also result from interband pairing, which is not shown here. Image adapted from [3].

The spin part of the wavefunction is described by a quantum number S, allowing for two different possibilities: either S = 0, which is *singlet pairing*, or S = 1, which is called *triplet pairing*. In a singlet pair, the electrons have opposite spin and therefore this is an anti-symmetric state, in Dirac notation: $\frac{1}{\sqrt{2}}(|\uparrow\downarrow\rangle - |\downarrow\uparrow\rangle)$. The triplet state is its symmetric counterpart, where the electrons are paired with equal spin, i.e., S = 1, which is divided in three options. Either the electrons have a finite spin projection along the quantization axis($|\uparrow\uparrow\rangle$ and $|\downarrow\downarrow\rangle$) or they have zero spin projection: $\frac{1}{\sqrt{2}}(|\uparrow\downarrow\rangle + |\downarrow\uparrow\rangle)$. *Conventional* superconductors are of singlet *s*-wave nature. The antipathy to magnetic fields, described in section 2.2, is clearly reflected in the opposite spin of the singlet pairs, since magnetic fields tend to align the spins in a solid. Generally, materials with a different pairing symmetry as classified as *unconventional*.

The concept of time asymmetry is less easily grasped at first sight. It is best understood mathematically. Therefore, we return to the anomalous Green's function. The class of superconductors characterized by an asymmetry in time, also called *odd-frequency* pairing, are classified by acquiring a minus sign under exchange of time variables:

$$f_{\alpha\beta,ab}(\boldsymbol{r}_1,\boldsymbol{r}_2,t_1,t_2) = -f_{\alpha\beta,ab}(\boldsymbol{r}_1,\boldsymbol{r}_2,t_2,t_1) \tag{2.15}$$

This means that naturally $f = 0$, when $t_1 = t_2$. Therefore, strictly spoken odd-frequency superconductivity is not a consequence of the Pauli exclusion principle. Instead, it

arises due to a constraint on the relative time coordinates of the anomalous Green's function. Yet it does allow for an electron pairing that is symmetric in momentum, spin and electron band that still meets the Pauli exclusion principle.

Pairing symmetry is an important topic in researching superconductivity, which is reflected in this thesis. For example, the pairing symmetry of the unconventional superconductor Sr_2RuO_4, which is the topic in Chapter 7, was thought to be equal-spin triplet *p*-wave for over 20 years. Only in 2020 this hypothesis was found to be unlikely, and currently, the pairing symmetry of Sr_2RuO_4 is a hotly debated topic: the proposals range from 'shadow-triplet' interband s+id-wave pairing to accidental degeneracies between *d*- and *g*-wave pairing[4, 5]. Another manifestation of triplet pairing will be encountered in Chapters 3 and 4, which discuss the proximity effect in a strong ferromagnet. Such superconducting correlations require spin-triplet pairing with finite spin ($|\uparrow\uparrow\rangle$ or $|\downarrow\downarrow\rangle$), exhibiting an odd time component to fulfill the anti-symmetry requirement. Before discussing the proximity effect in ferromagnets, I will introduce the superconducting proximity effect in normal metals in the next section.

2.4. THE PROXIMITY EFFECT AND JOSEPHSON JUNCTIONS

In section 2.1 omitted the space dependence of the superconducting condensate density, but naturally we can ask what governs this space dependence. For this we turn to the *first Ginzburg-Landau equation*, which reads in the absence of magnetic fields:

$$\alpha\psi + \beta|\psi|^2\psi + \frac{\hbar^2}{2m}\boldsymbol{\nabla}^2\psi = 0 \tag{2.16}$$

This equation is derived from minimizing the free energy associated with an order parameter (ψ) near a phase transition. The solution of Eq. 2.16 is expressed in exponential functions that contain a characteristic length scale ξ, called the *coherence length*, which is given in Ginzburg-Laundau theory as[4]:

$$\xi = \sqrt{\frac{\hbar}{2m|\alpha|}} \tag{2.17}$$

This length scale can be interpreted as the distance over which the density of the superconducting condensate can change its magnitude. Since the coherence length is finite, the magnitude of the condensate cannot fall to zero over an infinitesimally small

[4] In BCS theory, which I do not discuss in this thesis, the coherence length is defined as well. It signifies the typical length scale corresponding to the pairing interactions and is, therefore, sometimes explained as the average size of the Cooper pair.

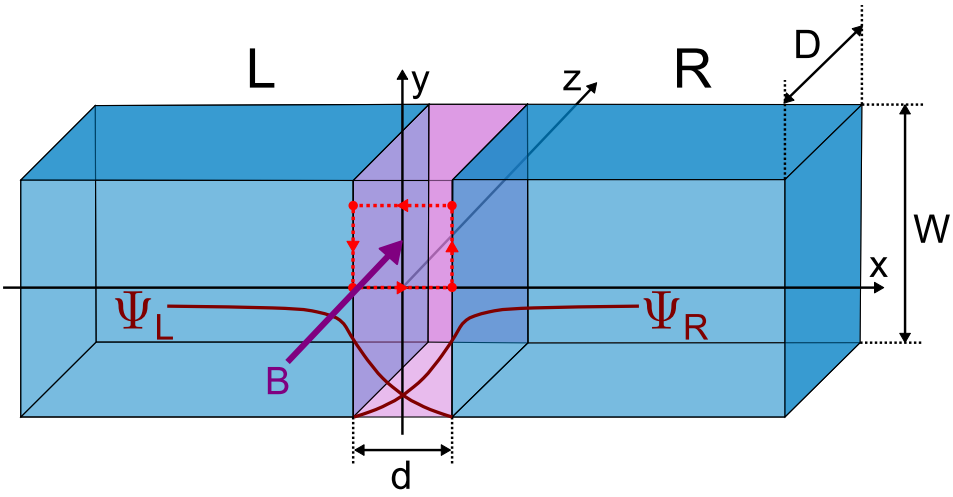

Figure 2.3: Schematic drawing of a Josephson junction: two superconducting leads (blue) separated by thin barrier layer of size d (pink). In dark red the amplitude of the superconducting wavefunctions is shown. As there is overlap between them, there can be a supercurrent flowing through the junction. A uniform magnetic field ($\boldsymbol{B} = B\hat{z}$) is applied to the junction, which results in an interference pattern observed in the critical current $I_c(B)$ (see section 2.6). This is calculated by computing a contour integral of the gauge covariant-phase gradient over the red dotted contour.

distance, like the interface between a superconductor and a non-superconducting material. Therefore, superconducting effects 'leak' into the material adjacent to the superconductor. This is known as the *superconducting proximity effect*.

The fact that a normal metal can show superconducting effects through the proximity effect raises the question whether a supercurrent can pass from one superconducting electrode to another if separated by a proximized material. The answer is yes, but only if the proximized material is thin enough to let the superconducting wave functions overlap. A sketch of such a geometry is given in Figure 2.3: two superconducting electrodes separated by a so-called *weak link* or *barrier*. This fundamental superconducting element is called a *Josephson junction* and forms the centerpiece of research on superconductors and their technological applications. Generally, the nature of the weak link determines the transport through the junction and can be insulating (I), normal metal (N), or ferromagnetic (F). A normal metal junction is denoted as an S−N−S junction. Chapter 4 will discuss S−F−S junctions; below, I will describe what drives the current through a Josephson junction.

If we assume that the coupling between the two electrodes is weak, the Cooper pair density of the electrodes remains largely unaffected. Instead, supercurrents in the weak link are driven by the gauge-invariant phase gradient, as is the case in the bulk of the superconductor. Specifically, when comparing the phase difference between two sides of the junction, we define the *gauge-invariant phase difference*, which is given by (omitting any z-dependence):

$$\varphi(y) = \int_{-d/2}^{d/2} \theta \, \mathrm{d}l = \gamma(-\frac{d}{2}, y) - \gamma(\frac{d}{2}, y) - \frac{2\pi}{\Phi_0} \int_{-d/2}^{d/2} A_x(x, y) \, \mathrm{d}x \tag{2.18}$$

Since we now know that the current through the junction is given by $\boldsymbol{J} = \boldsymbol{J}(\varphi)$, we can follow the arguments of Landau and Lifschitz to find a relation between the current and the gauge-invariant phase difference, aptly called the *current-phase relation*[6]. From Eq. 2.1 we see that the wavefunction is 2π-periodic in the electrodes. This is consequently transferred to the junction such that $\boldsymbol{J}(\varphi) = \boldsymbol{J}(\varphi + 2\pi)$. Furthermore, in the absence of any phase difference, no currents can be running, which means: $\boldsymbol{J}(2\pi n) = 0$, where n is an integer. Combined, this limits the current-phase relation to the following set of functions:

$$\boldsymbol{J} = \boldsymbol{J}_\mathrm{c} \sin\varphi + \sum_{m=2}^{\infty} \boldsymbol{J}_{\mathrm{c},m} \sin\big(m\varphi\big) \tag{2.19}$$

This current-phase relation is also known as the general formulation of the *first Josephson relation*, after Brian Josephson, who derived it when studying pair-wise tunneling in S−I−S junctions[7]. More commonly, in the case of weak coupling between the two electrodes, we can neglect the higher harmonics, and Eq. 2.19 is reduced to:

$$\boldsymbol{J} = \boldsymbol{J}_\mathrm{c} \sin\varphi \tag{2.20}$$

Here $\boldsymbol{J}_\mathrm{c}$ is the maximum current density the junction can sustain, called the *critical current density*. Above this current, a finite voltage is measured over the junction. This manifests itself as a *critical current* (I_c) during the measurement of the IV-characteristic of a junction, which is the most fundamental measurement of a Josephson junction, repeated many times throughout this thesis. In such measurement, a DC current is applied through the junction, and the voltage across the junction is recorded (see Figure 2.4). More technical details on obtaining IV-characteristics and the set-up used to gather the data presented in this thesis are provided in Appendix A. The remarkably simple result of Eq. 2.20 is yet another manifestation of macroscopic currents driven by the microscopic quantum mechanical phase, leading to junction properties that reveal the wave-like nature of the condensate. Two of those, I will review below.

2.5. SHAPIRO STEPS

In the previous section we found a relation between the current through a junction and the gauge-invariant phase difference over the junction. How is this related to an electric field applied to the junction? Electric (E)-fields can be written as a linear combination between a scalar potential (ϕ) and a vector potential ($\boldsymbol{A}$):

$$\boldsymbol{E} = -\frac{\mathrm{d}\boldsymbol{A}}{\mathrm{d}t} - \boldsymbol{\nabla}\phi \tag{2.21}$$

Also, from the time-dependent Schrödinger equation, one can show that the time evolution of the gauge covariant phase follows:

$$-\hbar\frac{\mathrm{d}\gamma}{\mathrm{d}t} = \frac{\mu_0\lambda_\mathrm{L}^2}{2n_\mathrm{s}}\boldsymbol{J}^2 + 2e\phi \tag{2.22}$$

This can be combined with Eq. 2.18, to obtain the time evolution of the gauge invariant phase difference:

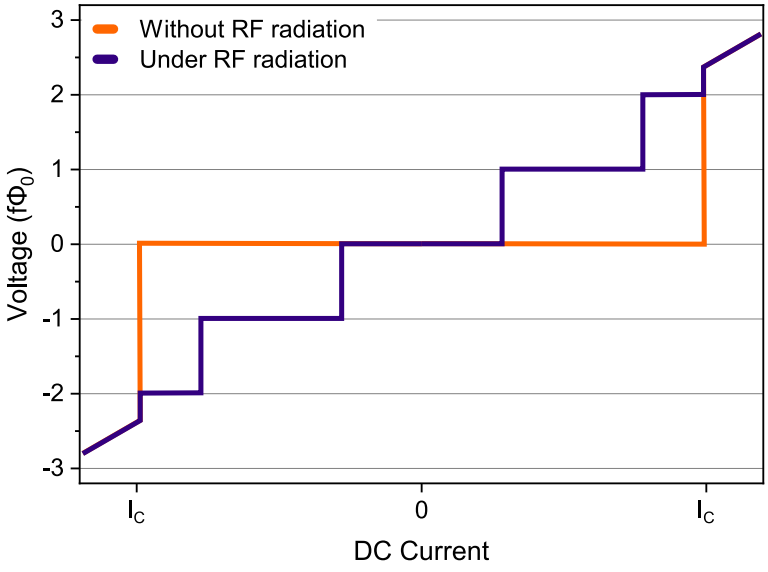

Figure 2.4: A schematic example of an IV-characteristic of a junction. If no microwave radiation is applied to the junction (orange curve), zero voltage is measured over the junction, as long as the current does not exceed the critical current I_c. Irradiation with RF-radiation results in quantized voltage steps that are spaced by $\Delta V = f\Phi_0$, which are called Shapiro steps. The measurement of a IV-characteristic is the most fundamental measurement in this thesis and is widely used to extract the critical current of Josephson junctions.

$$\frac{\mathrm{d}\varphi}{\mathrm{d}t} = -\frac{1}{\hbar}\left(\frac{\mu_0\lambda_\mathrm{L}^2}{2n_\mathrm{s}}\left(\boldsymbol{J}^2(\frac{d}{2}) - \boldsymbol{J}^2(-\frac{d}{2})\right) + 2e\phi\right) - \frac{2\pi}{\Phi_0}\int_{-d/2}^{d/2}\frac{\mathrm{d}A_x(x,y)}{\mathrm{d}t}\,\mathrm{d}x \tag{2.23}$$

Since the current is conserved in the junction ($\boldsymbol{J}^2(\frac{d}{2}) = \boldsymbol{J}^2(-\frac{d}{2})$), we can write:

$$\frac{\mathrm{d}\varphi}{\mathrm{d}t} = \frac{2\pi}{\Phi_0}\int_{-d/2}^{d/2} -\frac{\mathrm{d}\phi}{\mathrm{d}x} - \frac{\mathrm{d}A_x(x,y)}{\mathrm{d}t}\,\mathrm{d}x \tag{2.24}$$

Here we recognize the expression from Eq. 2.21 and we arrive at the *second Josephson equation*:

$$\frac{\mathrm{d}\varphi}{\mathrm{d}t} = \frac{2\pi}{\Phi_0}\int_{-d/2}^{d/2} E_x\,\mathrm{d}x = \frac{2\pi}{\Phi_0}V \tag{2.25}$$

The consequence of this equation is that a finite voltage V over the junction, entails a linear increase of the gauge invariant phase difference in time ($\varphi = \frac{2\pi}{\Phi_0}Vt$). Combining this with the current-phase relation, yields:

$$\boldsymbol{J} = \boldsymbol{J}_\mathrm{c}\sin\frac{2\pi}{\Phi_0}Vt \tag{2.26}$$

In other words, the application of a constant DC voltage yields an AC current through the junction with a frequency of $f = \frac{V}{\Phi_0}$, which translates to roughly 500 MHz per applied μV. The inverse of this effect can be encountered throughout this thesis. If a junction is irradiated with RF-radiation while driving a DC supercurrent through the junction, phase locking between the radiation and the supercurrents occurs. This results in a DC voltage over the junction, which appears as quantized steps in the IV-characteristic, spaced by $\Delta V = f\Phi_0$. These steps are called *Shapiro steps*; a schematic example of which is shown in Figure 2.4.

The measurement of Shapiro steps serves as definitive evidence for the Josephson effect without the use of static magnetic fields that might, for example, alter the magnetic texture of the S−F−S Josephson junctions presented in Chapter 4 and 5. Furthermore, they are conclusive proof of the emergence of spontaneous Josephson junctions in mesoscopic Sr_2RuO_4 structures, discussed in Chapter 7. Besides, the detection of Shapiro steps enables us to examine the periodicity of the current-phase relation. If the current-phase relation is not 2π periodic, for example, fractional Shapiro steps can be observed when it is dominated by a higher harmonic.

2.6. MAGNETIC INTERFERENCE IN A JOSEPHSON JUNCTION

One of the most fundamental measurements of a Josephson junction is the dependence of critical current on a magnetic field applied perpendicular to the junction (e.g., the y-direction or z-direction in Figure 2.3). Experimentally this is also known as superconducting quantum interferometry measurements, i.e., obtaining the $I_c(B)$-pattern of a junction. To calculate the expected $I_c(B)$, define a narrow rectangular loop of width d, with the bottom located at the origin and a height y (See the dotted contour in Figure 2.3). We integrate $\boldsymbol{\nabla}\gamma$ (using Eqs. 2.3 and 2.18) along this path to obtain[5]:

$$0 = \int_C \boldsymbol{\nabla}\gamma \, \mathrm{d}\boldsymbol{l} = -\varphi(y) + \varphi(0) + \frac{2\pi}{\Phi_0}\int_C \boldsymbol{A}\,\mathrm{d}\boldsymbol{l} + \frac{2\pi\mu_0\lambda_L^2}{\Phi_0}\left(\int_0^y J_{y,R}(\frac{d}{2}, y')\,\mathrm{d}y' + \int_y^0 J_{y,L}(-\frac{d}{2}, y')\,\mathrm{d}y'\right) \tag{2.27}$$

Using Stokes theorem, we can transform the integral over the vector potential into one over the magnetic field that penetrates the integration contour, resulting in the magnetic field flux ($\Phi = ydB$). Furthermore, in the case of a symmetric geometry: $J_{y,R}(\frac{d}{2}, y') = -J_{y,L}(-\frac{d}{2}, y')$. Therefore we find for $\varphi(y)$:

$$\varphi(y) = \varphi(0) + \frac{2\pi}{\Phi_0}\left(ydB + 2\mu_0\lambda_L^2\int_0^y J_{y,R}(\frac{d}{2}, y')\,\mathrm{d}y'\right) = \varphi(0) + \varphi_B \tag{2.28}$$

We recognize two parts in $\varphi(y)$: the first, $\varphi(0)$ is the phase difference at the origin. This can be thought of as the phase difference resulting due to a current or voltage bias between the two electrodes. The second, φ_B, results from the magnetic induction to the junction (see the inset of Figure 2.5). The current that runs along the junction might not be trivial to compute. However, in the case of a junction between two macroscopic superconducting leads, we have already found this quantity in the form of the Meissner effect (Eq. 2.11). At the boundary we have $J_{y,R}(\frac{d}{2}, y') = \frac{B\mu_0}{\lambda_L}$; filling in yields:

$$\varphi(y) = \varphi(0) + \frac{2\pi(2\lambda_L + d)B}{\Phi_0}y = \varphi(0) + \frac{2\pi L_{\mathrm{eff}}B}{\Phi_0}y \tag{2.29}$$

Where in the right-hand side we defined the *effective junction length* $L_{\mathrm{eff}} = 2\lambda_L + d$. We see that φ_B scales with fields penetrating the barrier and with fields penetrating the electrodes over a length scale λ_L on either side of the junction. Therefore L_{eff} can be considered as the length of the Josephson junction. Using the current-phase relation

[5] Actually $\int_C \boldsymbol{\nabla}\gamma\,\mathrm{d}\boldsymbol{l} = 2\pi n$, but we can set $n = 0$ if the current-phase relation is dominated by the first harmonic. In that case: $\sin(\varphi + 2\pi n) = \sin(\varphi)$.

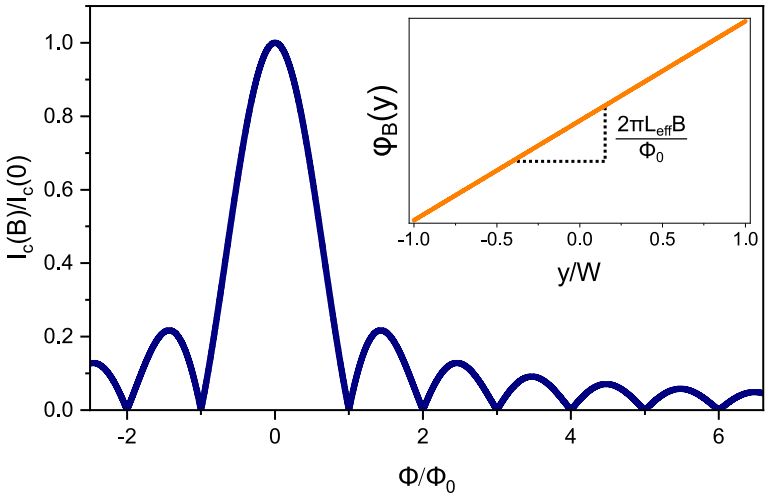

Figure 2.5: The interference pattern of the critical current in a Josephson junction due to the application of a field $I_c(B)$. This result corresponds to a typical Fraunhofer interference pattern commonly observed in optical diffraction patterns. The inset shows the gauge-invariant phase difference resulting from the magnetic induction to the junction, as a function of the length parameter running along the junction.

(Eq. 2.20), we can find the current that passes through the junction as a function of field:

$$I(B) = \int \boldsymbol{J}\,\mathrm{d}\boldsymbol{S} = \int_{-W/2}^{W/2} D J_c \sin\left(\varphi(0) + \frac{2\pi L_{\mathrm{eff}} B}{\Phi_0} y\right) \mathrm{d}y \tag{2.30}$$

For now we assume that the critical current density at zero field is distributed uniformly over the junction, yielding $J_c = \frac{I_c(0)}{DW}$. Also, note that $\varphi(0)$ is independent of y and therefore merely is a phase factor. Therefore, the critical current is reached if we current-bias the junction by setting $\varphi(0) = \pi/2$, from which follows:

$$\frac{I_c(B)}{I_c(0)} = \left| \frac{1}{W} \int_{-W/2}^{W/2} \cos\left(\frac{2\pi L_{\mathrm{eff}} B}{\Phi_0} y\right) \mathrm{d}y \right| = \left| \frac{\sin\left(\frac{\pi L_{\mathrm{eff}} W B}{\Phi_0}\right)}{\frac{\pi L_{\mathrm{eff}} W B}{\Phi_0}} \right| = \left| \frac{\sin\left(\frac{\pi\Phi}{\Phi_0}\right)}{\frac{\pi\Phi}{\Phi_0}} \right| \tag{2.31}$$

Here Φ is the total flux penetrating the junction. This result is the classic Fraunhofer pattern, obtained in an optical diffraction experiment of light waves in a single slit. I plot this result in Figure 2.5. Here we see a clear example of the wave-like nature of the condensate determining the macroscopic properties of the junction. As discussed below, measuring the magnetic interference pattern of the critical current is the ideal tool for understanding supercurrent transport in a Josephson junction.

2.7. EXTRACTING THE SUPERCURRENT DENSITY WITH FOURIER ANALYSIS

In the discussion so far, I assumed a uniform distribution of critical current throughout the weak link. In their 1971 paper, Dynes and Fulton [8] relax this criterion and discuss a relation between the shape of the SQI pattern and the supercurrent distribution in a junction. They realized that the current distribution in the junction can be extracted by complex inverse Fourier transform of $I_c(B)$. For simplicity, consider a J_c that only has a y-dependence, such that:

$$I(B) = \int \boldsymbol{J}\,\mathrm{d}\boldsymbol{S} = \left|\int_{-W/2}^{W/2} D J_c(y)\sin(\varphi(0)+\varphi_B)\,\mathrm{d}y\right| = \mathrm{Im}\left(e^{i\varphi(0)}\int_{-\infty}^{\infty} J_c(y)e^{i\varphi_B}\,\mathrm{d}y\right) \quad (2.32)$$

On the right-hand side, the integration bounds have been extended to infinity since there are no supercurrents outside the sample boundaries, and therefore the integral is zero. Besides, I dropped the D, so J_c can be considered as the critical current density per unit length. The critical current is given by the absolute value of the complex expression. Note that this equal to setting $\varphi(0) = \pi/2$ in Eq. 2.31.

$$I_c(B) = \left|\int_{-\infty}^{\infty} J_c(y)e^{i\varphi_B(B,y)}\,\mathrm{d}y\right| = |\mathfrak{I}_c| \quad (2.33)$$

From this equation a general expression for a Fourier transform can be recognized; conceptually depicted in Figure 2.6. For a junction with macroscopic leads discussed above, we have $\varphi_B(B,y) = \frac{2\pi L_{\mathrm{eff}} B}{\Phi_0} y$ and therefore:

$$I_c(\beta) = \left|\int_{-\infty}^{\infty} J_c(y)e^{2\pi i\beta y}\,\mathrm{d}y\right| \quad (2.34)$$

Here we have defined the reduced field $\beta = \frac{L_{\mathrm{eff}} B}{\Phi_0}$, such that the position along the junctions y and β form conjugate variables. The Fourier relation of Eq. 2.34, interestingly, gives rise to the possibility of extracting $J_c(y)$ by inverse Fourier transform of $I_c(B)$. This allows for studying the edge supercurrents in, for example, topological and semiconductor-based S−N−S junctions[9–12]. It also plays an important role in determining the rim currents in Chapter 4. In the next chapter, I will describe the technical details of the Fourier transform and its use to analyze experimental data. In light of the subject of this thesis, we are specifically interested in mesoscopically sized samples. Therefore we need to adjust the theory from this chapter first accordingly, which is the topic of the next chapter.

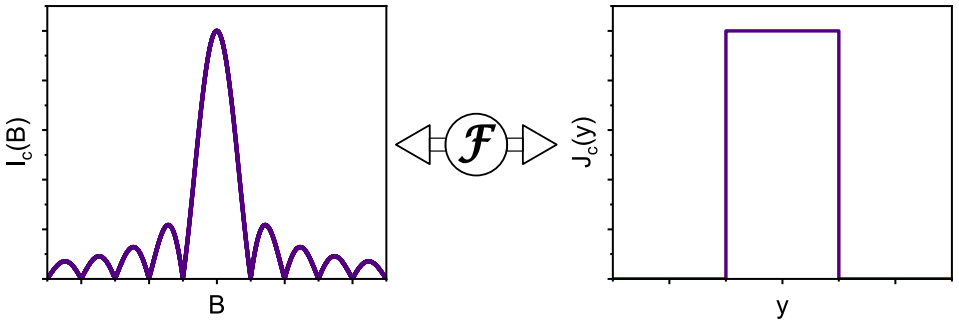

Figure 2.6: Conceptual representation of the Fourier relation between the magnetic interference pattern of the junction and the distribution of critical current density throughout said junction. For example, a uniform $J_c(y)$ leads to a Fraunhofer interference pattern. Practically, $I_c(B)$ is used to examine $J_c(y)$, which is a powerful tool to find possible current channels in a junction, when the interference pattern deviates from the Fraunhofer case.

APPENDICES

A. EXPERIMENTAL SET-UP AND MEASUREMENT PROCEDURE

The data presented in this thesis is acquired in an Oxford Instruments IntegraAC cryostat equipped with a vector magnet, aptly called the Vectormagnet. Since it features a vector magnet, it can apply a one Tesla magnetic field in any direction, and on top of that, it can reach a 6 T and 2 T magnetic field along two specified directions. The Vectormagnet is a 'wet cryostat,' having a dewar with liquid ^{4}He. It cools samples by letting in liquid ^{4}He in the cooling chamber. The spent helium is recycled and liquefied by the integrated pulse tube attached to the dewar. We have two different inserts (sample rods) for measurements: the high-T insert and the Heliox insert. The first is a home-built insert capable of reaching a 1.5 K base temperature, which is the base-T of the Vectormagnet sample chamber. The Heliox insert contains an inner vacuum chamber with an integrated ^{3}He system that is capable of reaching sub-300 mK temperatures. Finally, in both inserts, we can irradiate samples with RF radiation using an open-ended coax cable antenna placed in close proximity to the samples.

Considerable effort was put into the grounding of the Vectormagnet and its inserts. The entire system has a single ground connection to prevent ground loops; the rest of the physical or electrical grounds are decoupled by plastic o-rings and low-pass filters, respectively. The computer that controls the Vectormagnet is decoupled electrically from the measurement equipment by a purely optical data transmission system. To further reduce the electrical noise, only the measurement wire cores are used for measurements. The wire shields are always connected to the ground of the Vectormagnet.

Independent of the measurement insert, we have both DC and AC measurement equipment available. First, we can apply DC currents using a Keithley 6221 current source and obtain DC voltages using a Keithley 2182A volt meter. We can also obtain AC voltages using a Synktek MCL1-540 multichannel lock-in. The latter allows the simultaneous measurements of up to 6 AC voltages. Therefore, we can measure many samples at the same time. Besides, we can use the MCL1-540 in combination with a shunt resistor to generate a DC bias current that is superimposed on the AC current. Therefore, the Synktek lock-in can also be used to obtain IV-characteristics of the samples. In conclusion, using the equipment described above, we can measure voltages as a function of several parameters:

$$V(I_{\mathrm{DC}}, I_{\mathrm{AC}}, T, \boldsymbol{B}, f_{\mathrm{RF}}, P_{\mathrm{RF}}) \tag{2.35}$$

Here I_{DC} and I_{AC} are the applied DC and AC current, T is the sample temperature, $\boldsymbol{B}$ the applied magnetic field, f_{RF} is the frequency of the applied RF radiation, and P_{RF} the power of the applied RF radiation. In practice, we scan the parameter space with the Vectormagnet and use the measured voltages to extract the properties of our samples. For example, the resistance is defined using a DC measurement as:

$$R(I_{\mathrm{DC}}) = \frac{V_{\mathrm{DC}}(I_{\mathrm{DC}}) - V_{\mathrm{DC}}(-I_{\mathrm{DC}})}{2I_{\mathrm{DC}}} \tag{2.36}$$

Likewise, we establish the resistance using the lock-in as:

$$R(I_{\mathrm{AC}}) = \frac{V_{\mathrm{AC}}(I_{\mathrm{AC}})}{I_{\mathrm{AC}}} \tag{2.37}$$

Another example is the critical current (I_c) of a Josephson junction. It is defined as the current corresponding to a voltage measured over the junction that exceeds a certain threshold value (typically chosen just larger than the noise floor).

REFERENCES

[1] Gross, R. & Marx, A. Applied superconductivity: Josephson effect and superconducting electronics (2005). https://www.wmi.badw.de/teaching/lecture-notes (accessed: 28-2-22).

[2] Linder, J. & Balatsky, A. V. Odd-frequency superconductivity. *Rev. Mod. Phys.* **91**, 045005 (2019).

[3] Eschrig, M. & Löfwander, T. Triplet supercurrents in clean and disordered half-metallic ferromagnets. *Nat. Phys.* **4**, 138–143 (2008).

[4] Kivelson, S. A., Yuan, A. C., Ramshaw, B. J. & Thomale, R. A proposal for reconciling diverse experiments on the superconducting state in Sr_2RuO_4. *npj Quantum Mater.* (2020).

[5] Clepkens, J., Lindquist, A. W. & Kee, H.-Y. Shadowed triplet pairings in hund's metals with spin-orbit coupling. *Phys. Rev. Res.* **3**, 013001 (2021).

[6] Landau, L. D. & Lifschitz, E. M. *Course of theoretical physics Vol. 9: Statistical physics 2* (Pergamon Press, Oxford, UK, 1980).

[7] Josephson, B. Possible new effects in superconductive tunnelling. *Phys. Lett.* **1**, 251–253 (1962).

[8] Dynes, R. C. & Fulton, T. A. Supercurrent density distribution in Josephson junctions. *Phys. Rev. B* **3**, 3015–3023 (1971).

[9] Hart, S. *et al.* Induced superconductivity in the quantum spin Hall edge. *Nat. Phys.* **10**, 638–643 (2014).

[10] Huang, C. *et al.* Proximity-induced surface superconductivity in Dirac semimetal Cd_3As_2. *Nat. Commun.* **10**, 2217 (2019).

[11] Suominen, H. J. *et al.* Anomalous Fraunhofer interference in epitaxial superconductor-semiconductor Josephson junctions. *Phys. Rev. B* **95**, 035307 (2017).

[12] de Vries, F. K. *et al.* h/e superconducting quantum interference through trivial edge states in InAs. *Phys. Rev. Lett.* **120**, 047702 (2018).